NDT&E International 140 (2023) 102973

Contents lists available at ScienceDirect

NDT and E International

journal homepage: www.elsevier.com/locate/ndteint

Study on non-contact measurement method of resistance spot weld nugget diameter using laser ultrasonic technique

Kazufumi Nomura *, Shintaro Mishima, Soshi Deno, Tomokazu Sano

Graduate School of Engineering Osaka University, Japan

ARTICLE INFO

Keywords:
Laser ultrasonic
Resistance spot welding
Thin plate
Nugget diameter
Non-contact
Diffraction wave

ABSTRACT

Resistance spot welding can instantaneously join two or more plates by the resistance heating of the metal and is in high demand owing to its high productivity and high-work efficiency. For the quality control of resistance spot welding, the size and quality of the welded part, called the nugget, are important. Therefore, this study aims to establish a highly efficient and high-speed resistance spot-weld inspection method that can be applied to whole-lot inspection, which is currently a difficult process. The objective of this study is to measure the nugget diameter using laser ultrasonic technique that enable remote, non-contact ultrasonic inspection. An investigation of the available ultrasonic waves using simulated test specimens demonstrated the feasibility of estimating the distance from the generation/detection point to the joint using the diffraction of the Lamb wave, which can propagate long distances in a thin plate. By measuring the actual resistance spot welding specimens, it was determined that differences in the nugget diameter of approximately 0.5 mm could be clearly distinguished from the arrival time of the diffraction waves. It was also inferred that the nugget diameter could be calculated by determining the propagation velocity of the diffraction wave with a similar accuracy to that of the measurement using a contact-type probe.

1. Introduction

Welding is an essential technology in manufacturing, and there are demands for higher quality and efficiency in various applications. Resistance spot welding, which is widely used for joining thin plates, mainly in the automotive industry, can instantaneously join two or more plates by the resistance heating of the metal and is in high demand owing to its high productivity and high-work efficiency. However, several cases of destruction originate from the welded part; hence, high reliability is required.

For the quality control of resistance spot welding, the size and quality of the welded part, called the nugget, are important; in addition, various non-destructive inspections such as the hammer test are conducted. However, because products are often mass-produced, it is difficult to inspect all welded parts, and sampling inspection, in which a portion of the entire lot is sampled after welding, is often adopted [1]. It is impossible to guarantee that a sampling inspection does not contain defective products in a lot that has passed the inspection; therefore, the reliability of quality assurance is less than that of whole-lot inspection. Therefore, the establishment of a non-destructive inspection method that can inspect the entire number of lots is required to further improve the reliability of quality assurance. As aforementioned, resistance spot welding requires a short welding time and a large amount of welding work; hence, it is necessary to establish a non-destructive inspection method that is sufficiently efficient and fast to handle such welding work and conduct a whole-lot inspection. Some methods have been reported to monitor weld integrity based on the electrical output information generated during the resistance spot welding process [2–4]. However, because the criteria for such indirect inspections vary depending on the conditions, a method that can directly evaluate dimensions and defects is required.

To reduce carbon dioxide emissions, it is crucial to reduce the weight of automobile bodies; accordingly, the use of high-tensile steel plates [5] and resistance spot welding of dissimilar materials [6], such as steel-aluminum alloys [7], are being considered for this purpose. However, owing to the low deformation properties of the plate and the low toughness of the nugget, it is often difficult to perform a hammer test on high-tensile steel plates. In addition, owing to the formation of intermetallic compounds, it is also difficult to perform proper welding in resistance spot welding of dissimilar materials. Therefore,

* Corresponding author.
E-mail address: nomura@mapse.eng.osaka-u.ac.jp (K. Nomura).

https://doi.org/10.1016/j.ndteint.2023.102973
Received 22 August 2022; Received in revised form 21 August 2023; Accepted 12 October 2023
Available online 12 October 2023

non-destructive inspection methods that can inspect the entire number of lots are desirable.

As described above, a resistance spot welding inspection method that can be performed with high efficiency and speed is required. Potential inspection methods use X-ray [8–11], non-contact electromagnetic ultrasonic probe [12], air-coupled ultrasonic probe [13], thermography [14], and laser ultrasonic technique [15,16]. Because the X-ray method requires a large apparatus and lead shielding, it is limited by several challenges in its application; therefore, the ultrasonic method is considered to be beneficial for whole-lot inspection. Several conventional ultrasonic inspection methods for resistance spot welding [17–26] have been reported, in which a piezoelectric element is placed immediately above the nugget after welding to measure the weld. For example, Thornton et al. estimated the nugget diameter by using the phenomenon that ultrasonic waves excited from a probe placed on the upper plate surface pass through the nugget and are reflected from the lower plate bottom, resulting in multiple reflections [21]. Martin et al. also measured similar signals and reported a model to determine the state of nuggets using AI tools [22]. Ushijima et al. developed a spot-weld inspection robot [23] that combines robot control technology and an ultrasonic inspection device can perform the 3D imaging of the welded part's interior via the aperture synthesis method. However, these methods require the measurement device to be placed immediately above the nugget, making it difficult to handle the device. Similarly, Ji et al. have also constructed a robotic system using ultrasound, using a matrix phased array as a tool [24]. Takada et al. evaluated the nugget diameter by measuring Lamb waves, which are a type of plate wave transmitted through a nugget, using a piezoelectric element array [25]. This method can achieve an accuracy of ±0.5 mm by utilizing the fact that the attenuation of the Lamb wave transmitted via the nugget is larger than that of the base metal. However, the authors noted the problem of matching the array to curved surfaces for actual operations, which again raises the issue of handling measurement equipment. Xu et al. adopted the convergent air ultrasonic method to generate Lamb waves, which diffracted at the nugget and were observed at the backside of the transmitting position [26]. They evaluated the nugget diameter from the intensity distribution of these waves. Although this method enables a completely non-contact evaluation, the authors pointed out limitations such as low waveform intensity and low accuracy, which are addressed by scanning from multiple directions and averaging multiple received waveforms.

To address these problems, we focused on the laser ultrasonic technique, which enables remote, non-contact measurements by employing a laser as a probe. In the laser ultrasound technique, ultrasonic waves are generated by irradiating a pulsed laser onto the surface of the object to be measured, propagate through the interior and surface of the object, reflected at various interfaces, and detected by a laser interferometer, to obtain information. Compared to conventional ultrasonic methods, this method can generate high-frequency ultrasonic waves of up to several tens of MHz in a wide bandwidth, can be applied to narrow areas, owing to its small beam diameter, and can perform high-speed scanning using optical mirrors and mechanical stages because it is a non-contact method. In addition, compared to other noncontact ultrasonic methods, the measurement equipment can be placed farther from the object, and its signal-to-noise ratio is higher.

Currently, in addition to thickness measurements [27] and defect detection [28,29], the laser ultrasonic technique is adopted in various studies such as the evaluation of material properties, including phase transformation temperature [30] and residual stress [31]. As a representative example of the research on resistance spot welding, Kinoshita et al. identified the base metal, heat-affected zone, and molten part by visualizing the welding state of resistance spot welding specimens using frequency response analysis of waveforms obtained by the laser ultrasonic technique [32]. They reported that the results were discriminative, although sufficient resolution could not be obtained. However, this measurement was applied to a specimen after spot welding and after it had been destroyed; hence, it cannot be applied to whole-lot inspection. In TIG arc spot welding, which is similar to resistance spot welding, Nomura et al. applied an in-process laser ultrasonic technique during welding to determine the interfacial melting [33]. However, they reported the presence of inherent limitations, such as overlapping waveforms, in the measurement of the melting width and the commencement of melting, especially in the welding of thin plates with 2-mm thickness.

In this study, we attempted to measure the nugget diameter via a laser ultrasonic technique, to establish a highly efficient and high-speed resistance spot weld inspection method that can be applied to whole-lot inspections. Section 2 describes the adopted test specimen, experimental apparatus configuration, and measurement system. Section 3 describes the investigation of available ultrasonic waves using simulated specimens and the results of post-process measurements on resistance spot welding specimens. Finally, Section 4 presents the summary of this study.

2. Experimental arrangement

2.1. Test specimens

Resistance spot welding is a welding method primarily used for thin plates. In this study, we prepared seven types of test specimens, S_1–S_3, which were machined to simulate the overlapped joint condition of a thin plate, and R_1–R_4, which were welded by resistance spot welding.

In the machined test specimens, incisions were made from the left and right sides of 80 × 100 × 4 mm^3 and 80 × 100 × 10 mm^3 SUS304 plates, leaving a small portion in the center to simulate a straight joint with a constant width in the center. An outline of the adopted specimen is illustrated in Fig. 1 and the dimensions of each section are presented in Table 1. Two simulated joint widths, 2 mm for S_1 and 4 mm for S_2, were prepared to evaluate the effect of the simulated joint width on the measurement waveform. S_3 is ensured to be thicker than the other two, to check the effect of the plate thickness on the measured waveform.

In the resistance spot welding test piece, resistance spot welding was performed on two cold-rolled steel sheets (SPCC) of dimensions 80 × 150 × 1.2 mm^3. The dimensions of the nugget, which is the molten and solidified part, and that of the corona bonded part, which is the crimped part around the nugget, were modified by altering the welding pressure conditions and welding current during welding. Fig. 2 presents the appearance of specimen R_2 and a cross-sectional view of the area around the nugget obtained from another specimen prepared under the same conditions. The nugget and corona bond diameters were measured from these cross-sectional views and determined as the nugget and corona bond diameters for each specimen, as presented in Table 2.

2.2. Experimental apparatus and measurement systems

To measure the nugget diameter or the simulated bonding width, as described in Section 2.1 using the laser ultrasonic technique, it is necessary to evaluate the waveforms that can be obtained for various generation and detection configurations. Fig. 3 presents an overview of the laser ultrasonic measurement system adopted in this experiment.

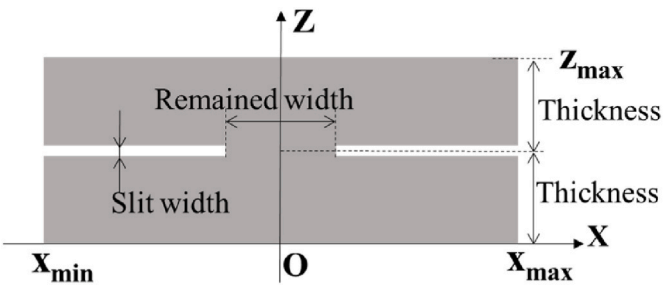

Fig. 1. Schematic diagram of machined specimen with slits from the sides.

Table 1
Dimensions of machined specimens.

Specimen	X_{max} [mm]	X_{min} [mm]	Z_{max} [mm]	Slit width [mm]	Thickness [mm]	Remained width [mm]
S_1	40	−40	4	0.3	2	2
S_2	40	−40	4	0.3	2	4
S_3	40	−40	10	0.3	5	2

The system was configured such that the generation laser was accessible from the backside of the test specimen and the detection laser was accessible from the front or back side of the specimen. Generally, laser ultrasonic techniques employ pulsed lasers for ultrasonic generation and laser interferometers for detection. The specifications of the generation and detection lasers are presented in Tables 3 and 4, respectively. A 1064 nm Nd:YAG laser (Nano L 90–100, Litron Lasers) was utilized as the generation laser, and a galvanometer scanner was used to enable multipoint irradiation, depending on the experimental conditions. There are two types of ultrasonic excitation modes excited by the laser: thermo-elastic and ablation[11]. In this study, the pulse energy and spot size were selected such that the ablation mode would be expected to exhibit intense ultrasonic excitation. The generation point of the laser was scanned using a galvano-mirror system to allow irradiation to any point on the backside of the specimen. A 532 nm Nd:YAG laser and a multichannel random quadrature interferometer based on Michelson interferometry (Quartet-1500, Bossa Nova) were adopted as detection lasers. Because the detection laser is transmitted by a fiber, the probe is portable, and the receiver probe can be mounted on a general-purpose robot arm, to allow movement on the surface or back side of the robot. To synchronize the timing of the start of the measurement by the detection laser with the timing of the generation laser irradiation, the irradiation of the transmission laser was detected using a photodetector, which was adopted as the trigger for the commencement of the measurement.

In this study, the A-scope, where the horizontal and vertical axes represent time and signal intensity, respectively, was obtained for each pulse of the generation laser from the propagation time of the ultrasonic wave excited at the transmission point and detected at the detection point. The B-scope, which color-modulates the A-scope and displays the position of the transmission point on the test specimen and the ultrasonic wave propagation time in Cartesian coordinates, was also obtained by scanning the transmission point for a single detection point, and the waves that can be used to evaluate the nugget diameter were elucidated based on these results.

3. Experimental results and discussion

3.1. Consideration of ultrasonic waves available in thin sheets

To achieve laser ultrasonic measurement of spot weld nugget diameters, we conducted a basic study on effective generation/detection laser arrangements and the types of waves that can be adopted for the

Table 2
Dimensions of RSW specimens.

Specimen	Thickness [mm]	Nugget diameter [mm]	Corona bond diameter [mm]
R_1	1.2	4.9	6.5
R_2	1.2	5.5	7.0
R_3	1.2	5.9	7.3
R_4	1.2	6.5	8.0

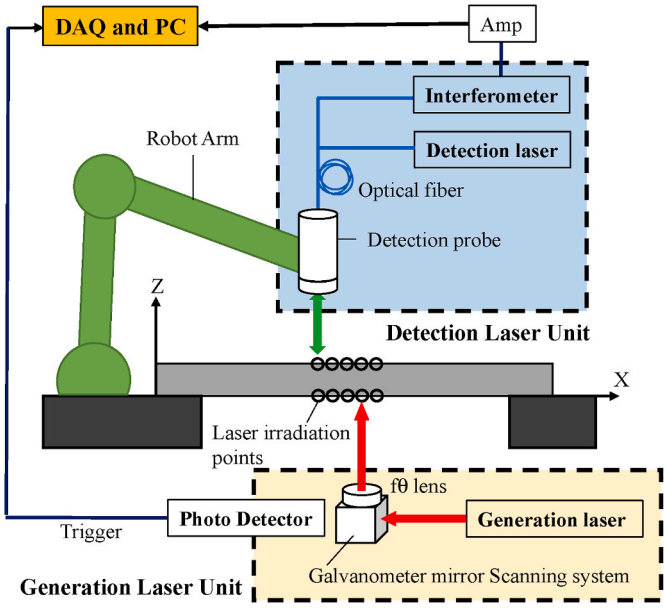

Fig. 3. Schematic diagram of experimental setup.

Table 3
Specifications of generation laser.

Laser	Nd:YAG
Wavelength	1064 nm
Repetition rate	100 Hz
Energy	40 mJ
Pulse width	8 ns
Beam spot diameter	1.5 mm

Table 4
Specifications of detection laser.

Laser	Nd:YAG
Wavelength	532 nm
Laser power	1 W
Detection range	100 kHz–50 MHz

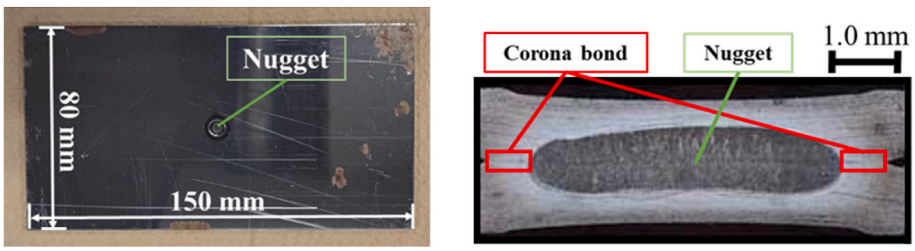

(a) Appearance (b) Cross section around the nugget

Fig. 2. Appearance of RSW specimen (R_2).

measurement. In spot welding, a thin plate with a thickness of 2 mm or less is often used. When laser ultrasonic measurement is applied to a thin plate, the ultrasonic waves propagating inside the plate behave like plate waves, and their behavior is quite complicated. In this section, the machining model described in Section 2.1 is adopted. To determine an effective generation/detection laser arrangement, experiments were conducted with two different laser arrangements, as illustrated in Fig. 4: (a) the same surface arrangement and (b) the opposite surface arrangement. In (a), the same surface arrangement, waves reflected from the edge around the simulated joint and from the surface of the plate are expected to be detected, while in (b), the opposite surface arrangement, waves diffracted at the simulated joint and those transmitted through the simulated joint are expected to be detected. The laser irradiation conditions are presented in Table 5, and the experiments were conducted on three types of mock-up specimens: S_1, S_2, and S_3. Considering the in-process and in-line applications, the laser irradiation point directly below the simulated welded part is difficult to use in practice because it is the location where the electrode for spot welding is positioned. However, we first conducted measurements using such a generation/detection arrangement because it is easy to consider the origin of the waves when considering an effective laser arrangement for each condition, as ultrasonic waves are continuously measured in space.

The B-scope results of the experiments are presented in Fig. 5. Figures (a)–(c) present the results of the same surface arrangement of the generation/detection lasers, which are expected to measure the waves reflected from the edges around the joint and the waves transmitted through the joint and reflected from the opposite surface. Fig. 5 (a) and (b) indicate that Lamb, edge-reflected, and shock waves were observed in the 2-mm thick test specimen. The shock wave propagates in the air near the surface of the specimen owing to the ablation phenomenon caused by the generation laser. The Lamb wave exhibits several amplitude peaks of similar intensity owing to its velocity dispersion. Fig. 5 (c) demonstrates that the number and time width of the amplitude peaks are narrower for the 5-mm thick specimen, thus indicating that the dispersion characteristics of the Lamb wave are diminished. However, the effect of the difference in the simulated joint width on the waveforms could not be verified from these waveforms, and it was difficult to evaluate the joint width from the waveforms obtained with the same surface arrangement.

Fig. 5 (d)–(f) present the results for the generation/detection laser opposite the surface arrangement. In this arrangement, the measurement of waves diffracted at the simulated joints from the same side ($X < 0$) as the receiving side ($X = -20$ mm) and the waves transmitted through the simulated joints from the opposite side ($X > 0$) of the detection ($X = -20$ mm) can be expected. Fig. 5 (d) and (e) demonstrate that the diffraction and transmission waves observed in the $X < 0$ and $X > 0$ ranges, respectively, were clearly observed for the 2-mm thick specimen. In particular, the diffracted waves seen at $X < 0$ have similar waveforms at various X positions in both simulated joint widths. Furthermore, diffraction waves were clearly observed even at a distance of $X = 20$ mm from the joint, thus suggesting that the diffraction waves could propagate for a certain distance within the thin plate. This feature is a major advantage in applications to actual structures, in-process, and in-line inspections, as it reduces restrictions on equipment placement. Fig. 5 (f) illustrates that the intensities of both the diffraction and transmission waves were considerably low for the 5-mm thick specimen. This is considered to be attributed to the fact that both the diffraction and transmission waves observed in this study are Lamb waves, and the characteristics of Lamb waves become weaker as the plate thickness increases. Spot welding is a welding method for thin plates with thicknesses of 2 mm or less; hence, the fact that diffraction waves are difficult to observe for thick plates is not considered to be a problem.

Table 5
Laser irradiation conditions.

Irradiation condition	Generation points				Detection point	
	X_s [mm]	X_e [mm]	Pitch ΔX [mm]	Points	X_d [mm]	Z_d [mm]
On the same surface	−15	20	0.5	71	−20	0
On the opposite surfaces	−20	20	0.5	81	−20	4/10

To investigate the application of diffraction waves based on the above results, the arrival time of the diffraction waves was checked to determine the extent to which it varies with the joint width. The arrival time of the diffraction waves is defined as the time when the diffraction waves exhibits a peak amplitude value in the vicinity of the observed diffraction wave on the A-scope. Because the diffraction waves we focused on were characterized by their long wavelength and distribution in the low-frequency band, we applied a bandpass filter that displays only the waves in the 0.3–0.8 MHz range to focus on this region. Fig. 6 presents the filtering results for Fig. 5 (d). Fig. 6 (a) presents the B-scope, while (b) illustrates the signal waveform on the A-scope at $X = -20$ mm in the vicinity where the diffraction wave is observed. Compared with the results in Fig. 5, the peak of the diffraction wave is clearer in the B-scope. For this signal, the arrival time of the diffraction wave is assumed to be 14.3 μs. The arrival time of the diffraction wave at $X = -10$ mm is 10.0 μs, which is faster than that at $X = -20$ mm, suggesting a diffraction wave propagation path, as illustrated in Fig. 7. Similar measurements were also performed for the wider joint specimen S_2 (Fig. 5 (e)), with similar results. Fig. 7 illustrates the difference in arrival time for the diffraction waves, which were earlier observed at 0.7–0.8 μs for the wider joint specimen S_2. Comparing specimens S_1 and S_2, the edge of the simulated joint was 1 mm closer to the generation/detection point for S_2, which indicates that the diffraction waves were diffracted at the edge of the simulated joint.

3.2. Evaluation by arrival time using diffraction waves

The experiment confirmed whether the nugget diameter could be evaluated from the arrival time of the diffraction waves using resistance spot welding specimens R_1–R_4. As illustrated in Fig. 8, the transmitting and receiving lasers were placed in an opposite surface arrangement at $X = -20$ mm and $X = +20$ mm, respectively; hence, the origin of the X- and Y-axes was located at the center of the nugget when the specimen

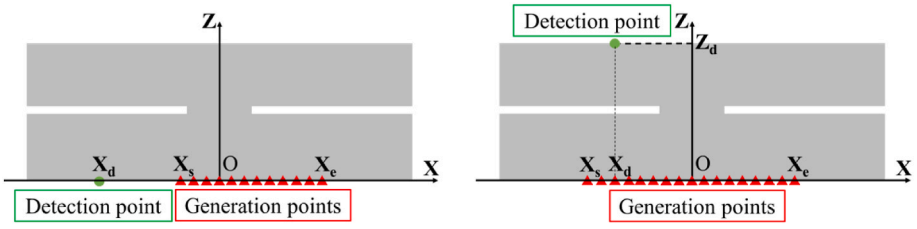

(a) Laser irradiation on the same surface (b) Laser irradiation on the opposite surfaces

Fig. 4. Schematic of LUT measurement for determining useful ultrasonic waves.

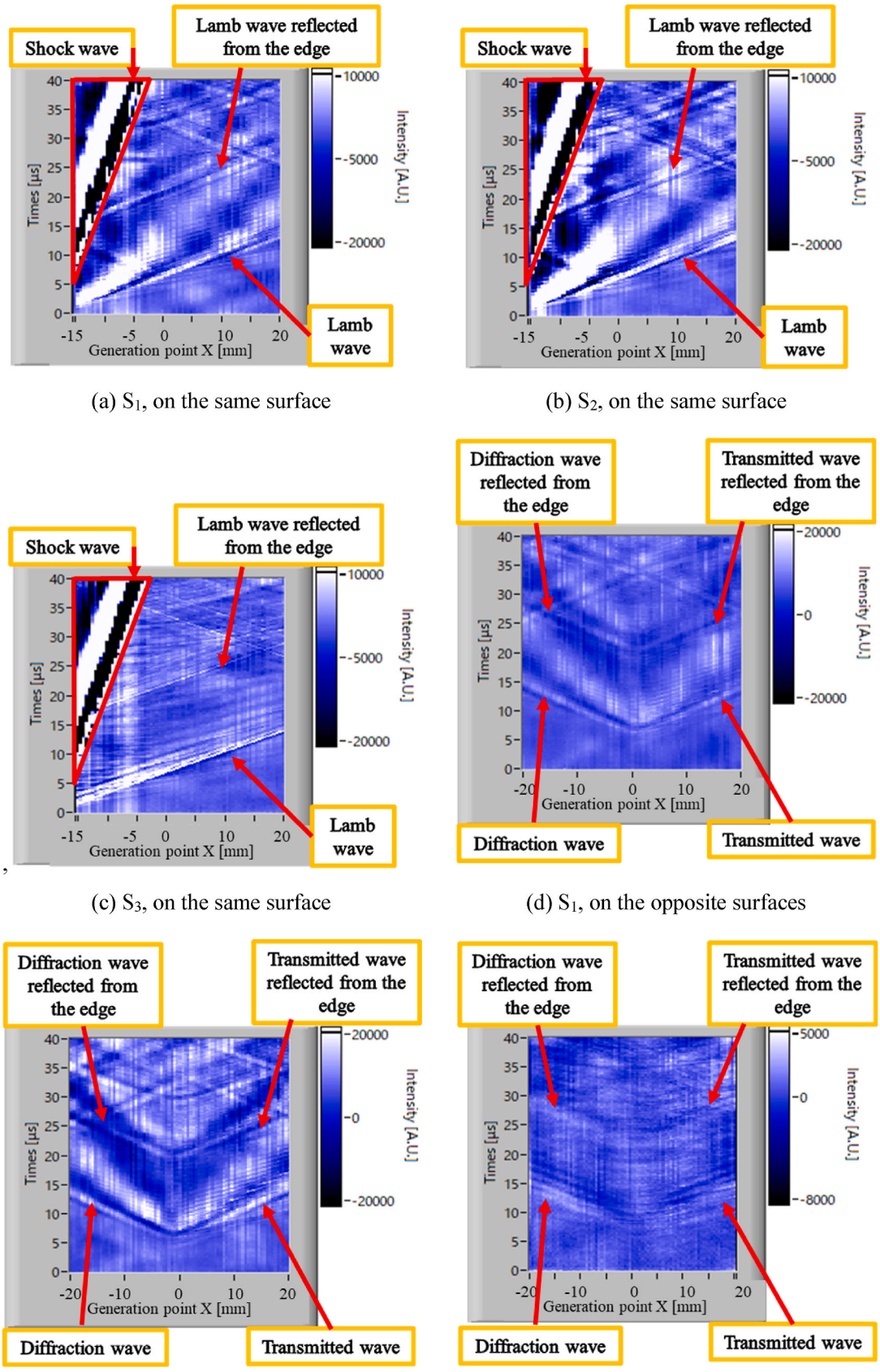

(a) S_1, on the same surface

(b) S_2, on the same surface

(c) S_3, on the same surface

(d) S_1, on the opposite surfaces

(e) S_2 on the opposite surfaces

(f) S_3 on the opposite surfaces

Fig. 5. B-scope results obtained from the LUT measurement.

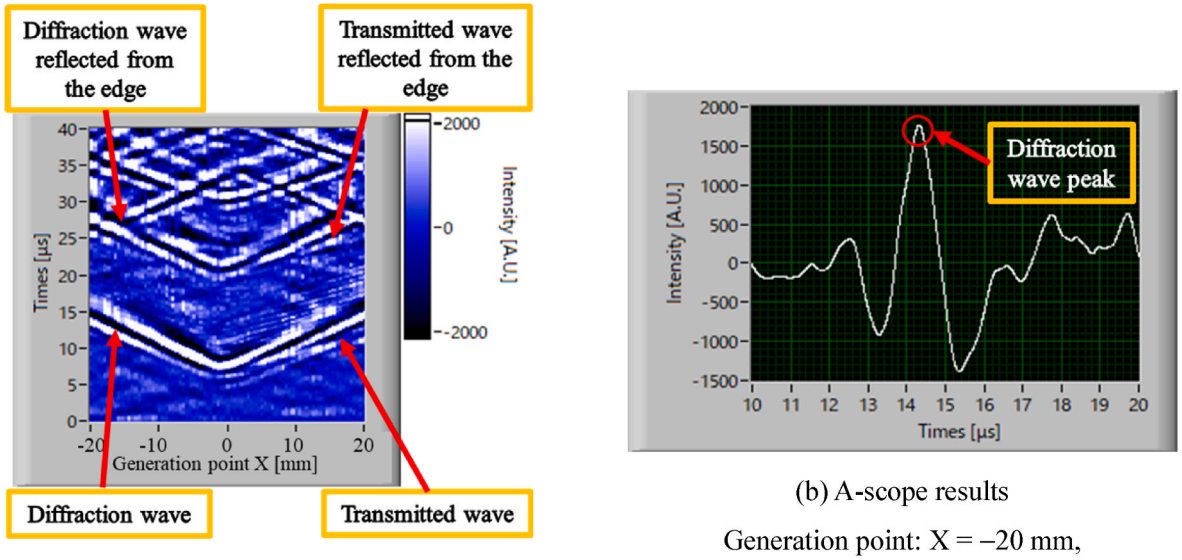

(a) B-scope results

(b) A-scope results
Generation point: X = –20 mm,
Detection point: X = –20 mm

Fig. 6. Results of the LUT measurement with 0.3–0.8 MHz filter to Fig. 5 (d) (S_1 on the opposite surfaces).

was viewed from above, as illustrated in Fig. 3 (a). However, a slight misalignment may occur. To minimize the measurement error due to misalignment, the generation/detection points were placed on opposite sides of the nugget, as illustrated in Fig. 8, and each point was measured separately. This allows the nugget diameter measurement to be compensated by summing the left and right measurements, even if there is a misalignment in the left and right directions.

Fig. 9 presents the A-scope obtained at X = −20 mm for specimens R_1 and R_4 as examples of the measurement results; accordingly, it is inferred that characteristic diffraction waves are observed in the resistance spot welding specimens and mock-up specimens presented in Fig. 6. Table 6 presents the arrival times of the diffraction waves at X = −20 mm and X = +20 mm for each specimen and the sum of these arrival times. Measurements were taken three times for each specimen and each point, and the results are shown as averages. The total arrival time of the diffraction waves decreases as the nugget diameter increases. This result is logical, as the propagation distance of the diffraction waves is expected to decrease as the nugget diameter increases. Fig. 10 illustrates this result by plotting the total diffraction arrival time at X = −20 mm and X = +20 mm for each specimen on the vertical axis, and the nugget diameter of the specimen on the horizontal axis. It can be observed that a significantly strong negative correlation is obtained between the diffraction arrival time and the nugget diameter of the specimens. Hence, using the arrival time, this method can be easily applied to the actual measurement of the nugget diameter.

3.3. Calculation of nugget diameter

In Section 3.2, we demonstrated that there is a correlation between the arrival time of the diffraction waves and the actual nugget diameter, and we investigated the possibility of calculating the nugget diameter from the arrival time of the diffraction waves. To investigate the velocity of diffraction waves observed in this study, the measurements described in Section 3.2 were performed on resistance spot welding specimens R_1–R_4 for X = −30 mm and +30 mm; in addition, the difference in propagation paths, as illustrated in Fig. 11, was used to calculate Equation (1) and obtain the diffraction wave velocity for each specimen. The diffraction wave velocity v_d^i was obtained for each specimen under the generation/detection conditions, as illustrated in Fig. 11.

$$v_d^i = \frac{20 \times 10^{-3}}{t_{\pm 30}^i - t_{\pm 20}^i} \ [\mathrm{m/s}] \tag{1}$$

where $t_{\pm 30}^i$ denotes the arrival time of the diffraction waves at X = −30 mm and +30 mm for each specimen and $t_{\pm 20}^i$ denotes the arrival time of the diffraction waves at X = −20 mm and +20 mm. As in Section 3.2, measurements were taken three times for each specimen and each point, and the results are shown as averages. The measurement results for $t_{\pm 30}^i$ and the calculation results for v_d^i are presented in Table 7. In laser ultrasonic measurements where the generation/detection conditions other than the position do not change, as in the experiments in this study, the velocity of the Lamb wave, whose velocity is determined by *fd*, the product of the frequency *f* and the plate thickness *d*, is considered to be unaltered. Therefore, the velocity under each condition was averaged to obtain the diffraction wave velocity v_d = 2720 m/s.

The nugget diameter was calculated from the diffraction wave velocity and arrival times of the measurements taken at X = −20 mm and +20 mm, as described in Section 3.2. Assuming the propagation path presented in Fig. 12, the nugget diameter $\Phi^i = r_1^i + r_2^i$ was calculated for each specimen using Eqs. (2) and (3).

$$r_1^i = 20 \times 10^{-3} - L_1^i = 20 \times 10^{-3} - \frac{t_{-20}^i v_d}{2} \ [\mathrm{m}] \tag{2}$$

$$r_2^i = 20 \times 10^{-3} - L_2^i = 20 \times 10^{-3} - \frac{t_{+20}^i v_d}{2} \ [\mathrm{m}] \tag{3}$$

Table 8 presents the results of the nugget diameter calculations, while Fig. 13 illustrates a plot of the calculated and actual nugget diameters on the vertical and horizontal axes, respectively. The error of the calculated nugget diameter is approximately ±0.5 mm, which is comparable to the accuracy of previous studies using contact-type probes [25].

3.4. Discussion

Which Lamb wave propagation mode of the diffracted waves evaluated in this study is considered here. Lamb waves generally exhibit complex multimodal and dispersive behavior, expressed by the Rayleigh-Lamb frequency equation [36]. In this study, we used software [37] to calculate the dispersion curve of Lamb waves in an SPCC plate

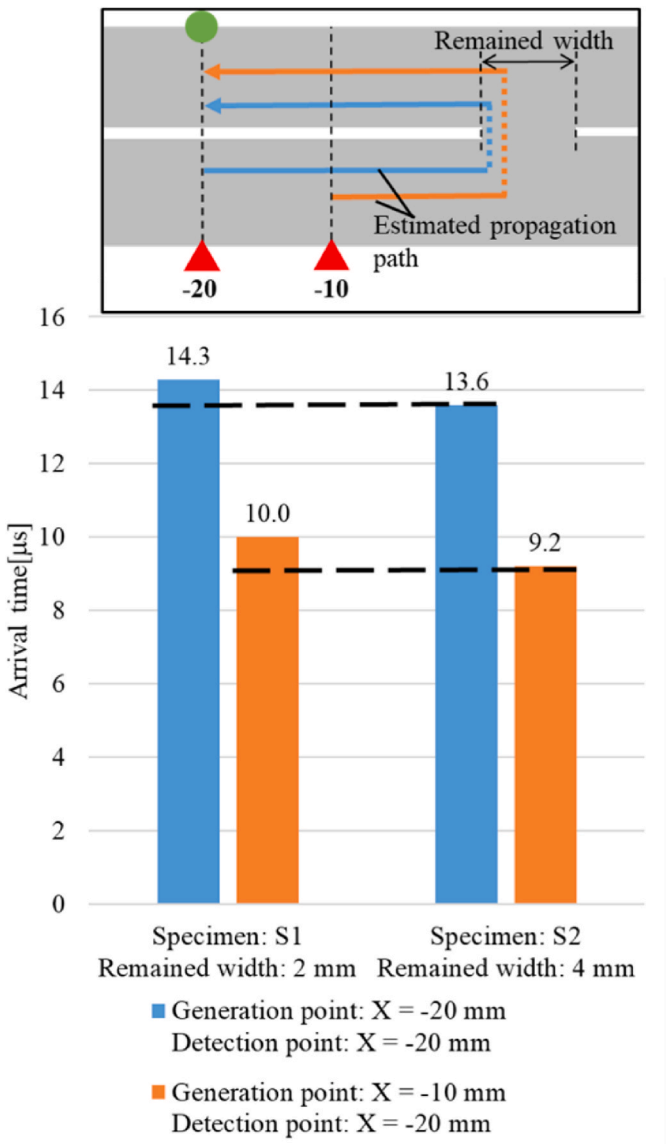

Fig. 7. Arrival time comparison of the diffraction wave.

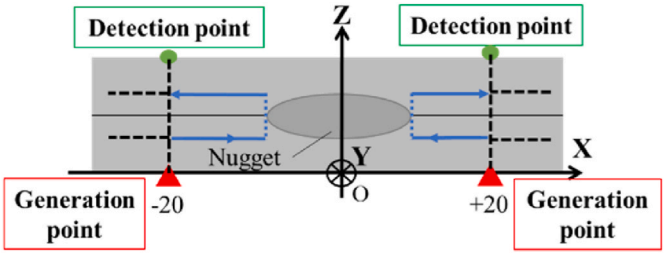

Fig. 8. Schematic diagram of LUT measurements for RSW specimens.

(longitudinal wave velocity: 5900 m/s, transverse wave velocity: 3200 m/s) with a thickness of 1.2 mm. The calculation result shows that only low-order modes of A_0 and S_0 exist in the 0.3–0.8 MHz region. Focusing on 0.5 MHz as a representative, the group velocity in A_0 mode is 3044 m/s, which is close to the velocity of 2720 m/s calculated in Section 3.3, although there is a difference of about 10 %. Therefore, the diffracted waves evaluated in this study are considered to be dominated by the A_0 mode component of the Lamb wave.

In this method, the arrival time of the diffraction waves is defined as the time when the amplitude reaches its maximum peak value near the point where the diffraction wave is observed. However, as illustrated in the A-scopes of Figs. 6 and 9, multiple peaks with large amplitudes are observed near the maximum amplitude peak value, and the timing of evaluation is often not very clear. If the arrival time is determined using the peak next to the peak that should be evaluated on the A-scope, a difference of approximately 1 μs is generated, and this difference is approximately 0.5 mm in nugget diameter; hence, the effect cannot be ignored. In this measurement, the peaks obtained by the B-scope, which is spatially continuous visual information, were relatively clear; therefore, there was no significant problem in determining the signal. However, for actual applications in production, it will be necessary in the future to determine signal processing and laser generation/detection conditions that will make it easier to distinguish diffraction peaks. Since the Hilbert transform can obtain the waveform envelope, it can be an effective method for determining the arrival time of diffracted waves.

In Section 3.2, we mentioned that the deviation in the x direction is canceled by summing the time at the left and right measurements, and the effect is small. Here, we consider the displacement in the y direction. Fig. 14 is a simplified diagram assuming a nugget diameter of Φ4.9 mm and a generation/detection position of X = −20 mm. Simple geometrical calculation shows the Lamb wave from the laser irradiation point propagates 17.55 mm to the edge of the nugget. Here, consider that the irradiation point is deviated by 1 mm in the y direction (the figure is exaggerated for clarity). The error is +0.03 mm for the expected propagation distance at this deviation. Therefore, the error caused by the displacement in this direction is quite small.

This method primarily targets resistance spot welding. In resistance spot welding, there is a corona bond part crimped by the electrode pressure around the nugget part, which is the molten solidified part. Because nugget diameter is an important parameter for the strength of resistance spot welding, an inspection method that can calculate the net nugget diameter without corona bond is required[17]. Table 2 shows that for the specimens used in this study, the diameter of the corona bond part is about 1.5 mm larger than the nugget diameter. However, Table 8, Fig. 13 shows that the calculated results have an error of about ±0.5 mm from the actual nugget diameter, so it is unlikely that the diffraction waves at the corona bond part are captured. Nevertheless, at this stage, it is not possible to deny physical phenomena such as diffraction at the corona bond or, conversely, diffraction after penetrating the nugget within a short distance (less than the wavelength of Lamb wave). Therefore, experimental verification focusing on the difference in the corona bond should be conducted. It is difficult to verify only the effect of the corona bond because the corona bond also becomes larger as the nugget diameter increases, owing to the nature of spot welding in the present specimen. To verify this assertion, it is necessary to prepare a resistance-spot test specimen made of a high-tensile steel plate, which has a smaller corona bond, and examine the effect of the corona bond.

We considered the applicability of this method to in-process measurements. In this measurement method, the generation/detection device is non-contact, and the electrode located directly above and below the welded part can be physically avoided. In addition, the method does not require waveform averaging, and only a single shot of generation/detection information is required to obtain a result, thus enabling a fast measurement. Furthermore, in-process measurement, in which welding and measurement are performed simultaneously, is possible. Depending on the repetition frequency of the laser, it may be possible to capture the joint behavior during a significantly short spot-welding process. However, such in-process measurements must be performed when the nugget is molten or when the area around the nugget is extremely hot. Studies have reported the fundamental behavior of ultrasonic waves, such as the velocity and attenuation of longitudinal and transverse waves, when ultrasonic waves are excited by a laser in steel materials in the temperature range from 17 to 1200 °C [34]. Studies have also reported in which Lamb waves reflected by defects were identified, when ultrasonic

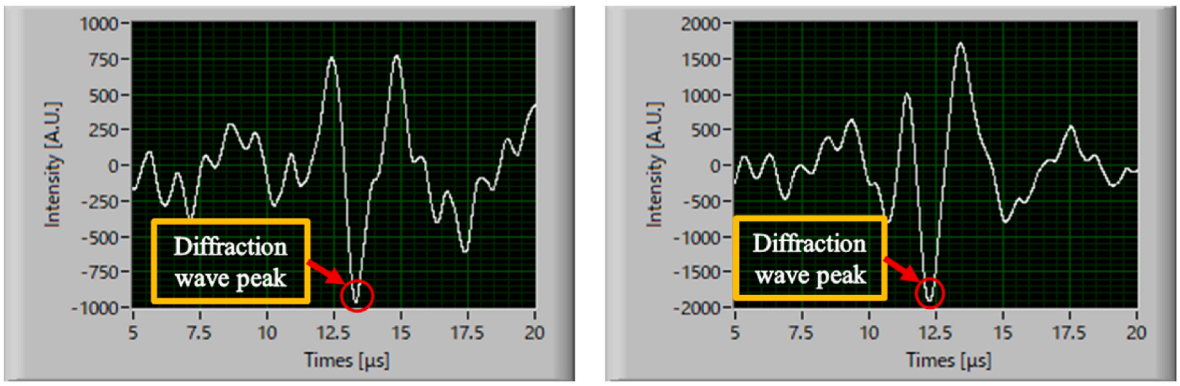

(a) R_1 (Nugget diameter: 4.9 mm) (b) R_4 (Nugget diameter: 6.5 mm)

Fig. 9. A-scope result of LUT measurement for RSW specimen where the generation and detection points are both X = −20 mm.

Table 6
Arrival times of diffraction wave.

Specimen (Nugget diameter [mm])	Arrival time [μs] Generation and Detection point: X = −20 mm	Arrival time [μs] Generation and Detection point: X = +20 mm	Total arrival time [μs]
R_1 (4.9)	13.2	12.7	25.9
R_2 (5.5)	12.8	12.8	25.6
R_3 (5.9)	12.4	12.2	24.6
R_4 (6.5)	12.3	12.0	24.3

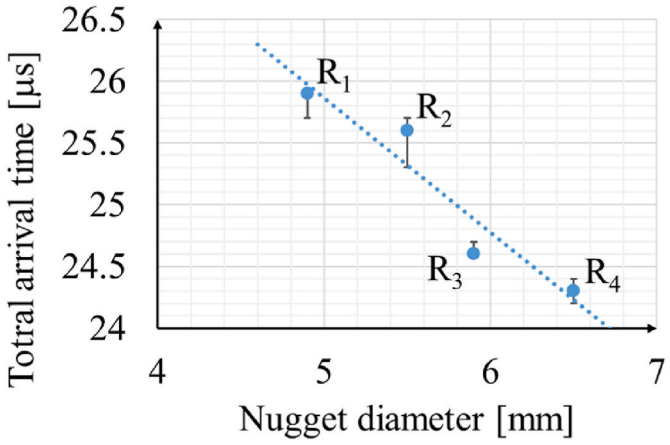

Fig. 10. Relationship between total arrival time of diffraction wave and nugget diameter.

waves are excited by a laser in SiC plates at 1000 °C [35]. However, the fundamental behavior at higher temperatures and that of the Lamb waves in steel utilized in this method are yet to be elucidated. Therefore, a fundamental investigation of laser ultrasonic phenomena at high temperatures and under conditions including melting is necessary to realize actual in-process measurements. However, resistance spot welding is a process in which the welded part solidifies and cools almost instantaneously. Regardless of the difficulty of in-process measurements owing to their ultrasonic behavior and other factors, in-line measurement, in which measurement is performed immediately after welding to determine quality, is considered relatively easy to achieve.

4. Conclusion

In this study, we measured the nugget diameter of a spot weld of a

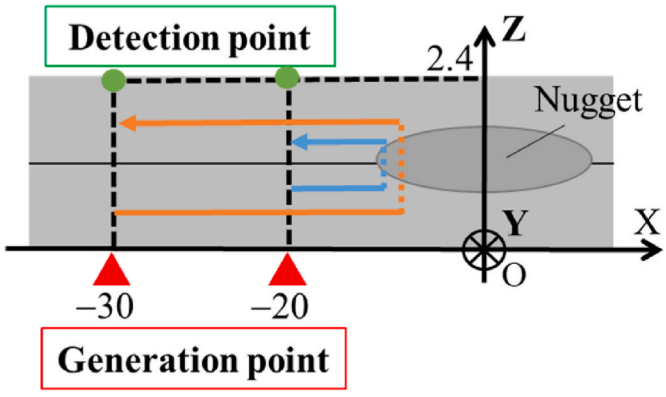

Fig. 11. Schematic diagram of LUT measurement for calculating diffraction wave speed.

Table 7
Calculation results for diffraction wave speed.

Specimen (Nugget diameter [mm])	Arrival time t^i_{-30} [μs]	Arrival time t^i_{+30} [μs]	Diffraction wave speed $v^i_{-30,-20}$ [m/s]	Diffraction wave speed $v^i_{+30,+20}$ [m/s]
R_1 (4.9)	20.3	20.3	2820	2610
R_2 (5.5)	19.7	20.2	2900	2710
R_3 (5.9)	19.5	19.9	2830	2600
R_4 (6.5)	19.3	20.1	2870	2460

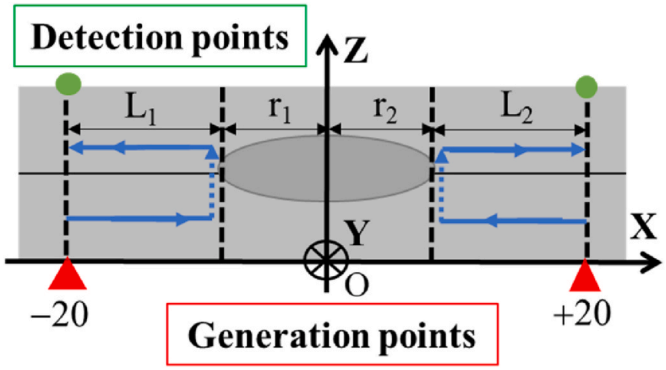

Fig. 12. Estimated propagation path of diffraction wave.

Table 8
Calculation results of estimated nugget diameter.

Specimen (Nugget diameter [mm])	Estimated nugget diameter [mm]
R_1 (4.9)	4.87
R_2 (5.5)	5.27
R_3 (5.9)	6.50
R_4 (6.5)	6.96

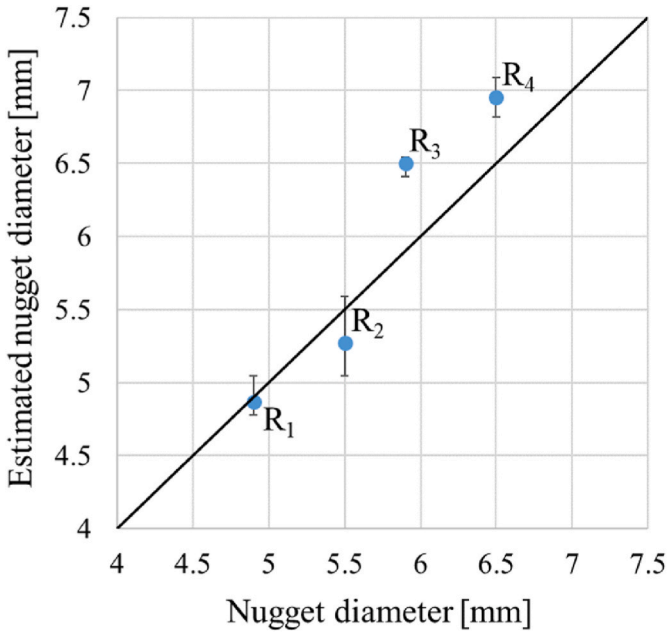

Fig. 13. Relationship between nugget and estimated nugget diameters.

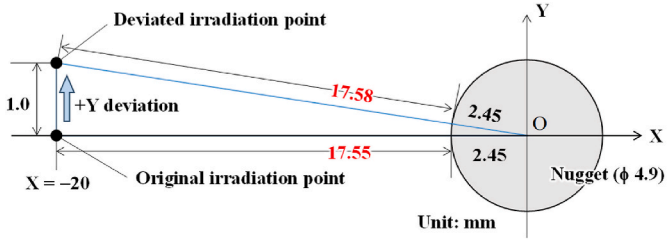

Fig. 14. Evaluation of the effect of irradiation position deviation in the y-axis (Exaggerated for easier understanding).

thin plate using a laser ultrasonic system that enables remote, non-contact ultrasonic inspection. First, we adopted a mock-up of a joint between two thin plates, and demonstrated that the distance from the generation/detection point to the joint can be estimated by using the diffraction of Lamb waves, which can propagate long distances within the thin plates. Next, by measuring the actual resistance spot-welded specimens, we demonstrated that differences in the nugget diameter of approximately 0.5 mm can be clearly distinguished from the arrival time of the diffraction waves. We also demonstrated that the nugget diameter could be calculated by determining the propagation velocity of the diffraction wave with an accuracy close to that of the measurement using a contact-type probe.

Author statement

Kazufumi NOMURA: Conceptualization, Methodology, Software, Investigation, Resources, Data Curation, Writing - Original Draft, Writing - Review & Editing, Visualization, Supervision, Project administration, Funding acquisition, Shintaro MISHIMA: Conceptualization, Methodology, Validation, Investigation, Resources, Data Curation, Writing - Original Draft, Visualization, Soshi DENO: Resources, Data Curation, Visualization, Tomokazu SANO: Resources, Supervision, Project administration, Funding acquisition.

Declaration of competing interest

The authors declare that they have no known competing financial interests or personal relationships that could have appeared to influence the work reported in this paper.

Data availability

The data that has been used is confidential.

Acknowledgments

The resistance spot welding specimens were prepared by the materials joining engineering laboratory of the Osaka Institute of Technology. We would like to express our gratitude to them.

References

[1] Tanishiki H, Mochizuki M. Development of automatic ultrasonic examination system for spot welding. in Preprints of the National Meeting of JWS 2011;2011s. 74–74.
[2] Kihara H, Otsuka H, Terasaki H, Komizo Y, Fukui K. Real time quality assessment in resistance spot welding process. in Preprints of the National Meeting of JWS 2012; 2012s:250–1.
[3] Zhou K, Yao P. Overview of recent advances of process analysis and quality control in resistance spot welding. Mech Syst Signal Process 2019;124:170–98.
[4] Lee J, Noh I, Jeong SI, Lee Y, Lee SW. Development of real-time diagnosis framework for angular misalignment of robot spot-welding system based on machine learning. Procedia Manuf 2020;48:1009–19.
[5] Takada H, Kitagawa M, Hirose T, Ikeda R, Nishimura K. Highly reliable nondestructive testing technique for spot-welds in automotive bodies assembled from high tensional steel parts. Materia Japan 2009;48:79–81.
[6] Krishnan V, Ayyasamy E, Paramasivam V. Influence of resistance spot welding process parameters on dissimilar austenitic and duplex stainless steel welded joints. Proc IME E J Process Mech Eng 2021;235(1):12–23.
[7] Tanaka K, Fukahori M, Nishiguchi K. Aluminum/steel resistance spot welding process for multi-material car body. J Jpn Weld Soc 2021;90:497–500.
[8] Kato K. The most up-to-date radiographic examination technology. J Jpn Weld Soc 2001;70:646–9.
[9] Morisada Y, Imaizumi T, Fujii H. Clarification of defect formation mechanism in friction stir welding by X-ray radiography. J Jpn Weld Soc 2014;32:31–7.
[10] Madani S, Azizi M. Detection of weld defects in radiography films using image processing. Sci J 2015;36(3):2397–404.
[11] Yaping L, Weixin G. Research on X-ray welding image defect detection based on convolution neural network. J Phys Conf 2019;1237:032005.
[12] Hernandez-Valle F, Dixon S. Initial tests for designing a high temperature EMAT with pulsed electromagnet. NDT E Int 2010;43:171–5.
[13] Gan TH, Hutchins DA. Air-coupled ultrasonic tomographic imaging of high-temperature flames. IEEE Trans Ultrason Ferroelectrics Freq Control 2003;50: 1214–8.
[14] Runnemalm A, Ahlberg J, Appelgren A, Sjökvist S. Automatic inspection of spot welds by thermography. J Nondestr Eval 2014;33(3):398–406.
[15] Scruby CB, Drain LE. Laser ultrasonics techniques and applications. CRC Press; 1990.
[16] Hutchins DA. 2 - ultrasonic generation by pulsed lasers. In: Mason WP, Thurston RN, editors. Physical acoustics, 18 21–123. Academic Press; 1988.
[17] Yokohama S, Braconnier D, Dao G, Carcreff E. FMC/TFM, the latest ultrasound testing technologies. J Jpn Weld Soc 2019;88:96–9.
[18] Zhao X, Zhang YS, Chen GL. Ultrasonic fast identification of automotive body spot weld defect based on echo characteristics qualitative analysis. Sci Technol Weld Join 2006;11:731–6.
[19] Denisov AA, Shakarji CM, Lawford BB, Maev R Gr, Paille JM. Spot weld analysis with 2D ultrasonic arrays. J Res Natl Inst Stand Technol 2004;109:233–44.
[20] Satonaka S, Nishi K, Nishiwaki T, Kohno Y. Ultrasonic evaluation of spot welds by local immersion method. J Jpn Weld Soc 1997;15:58–63.
[21] Thornton M, Han L, Shergold M. Progress in NDT of resistance spot welding of aluminium using ultrasonic C-scan. NDT E Int 2012;48:30–8.
[22] Martín Ó, Pereda M, Santos JI, Galán JM. Assessment of resistance spot welding quality based on ultrasonic testing and tree-based techniques. J Mater Process Technol 2014;214(11):2478–87.
[23] Ushijima A, Saito M, Matsumoto S. Spot welding inspection robot achieving labor saving and improvement of reliability using 3D ultrasonic inspection equipment. Toshiba Rev 2019:74 25–28.

[24] Ji C, Na JK, Lee Y-S, Park Y-Do, Kimchi M. Robot-assisted non-destructive testing of automotive resistance spot welds. Weld World 2021;65:119–65.
[25] Takada H, Ozeki T, Ikeda R, Hirose T. Ultrasonic method for testing spot-welds. J. Japan Instit. Metals Mater. 2012;76:555–62.
[26] Xu C, Ihara I. Non-contact evaluation of spot-welded nugget size based on measuring diffracted Lamb waves by focused air-coupled ultrasound. Transact. Japan Soc. Mech. Eng. 2015;81. 15-00107-15–00107.
[27] Izumi Y, Akamatsu S, Takahashi I. Thickness measurement for steel by the laser ultrasonic method. In: Dynamics & design conference 2006; 2006. 258-1 - 258-4.
[28] Ochiai M, et al. Sizing of micro cracks using laser-induced broad-band surface waves. J Atom Energy Soc Jpn 2001;43:275–81.
[29] Tian Z, Howden S, Ma Z, Xiao W, Yu L. Pulsed laser-scanning laser Doppler vibrometer (PL-SLDV) phased arrays for damage detection in aluminum plates. Mech Syst Signal Process 2019;121:158–70.
[30] Zamiri S, et al. Laser ultrasonic velocity measurement for phase transformation investigation in titanium alloy. In: 2013 IEEE international ultrasonics symposium (IUS); 2013. p. 683–6. https://doi.org/10.1109/ULTSYM.2013.0176.
[31] Karabutov A, et al. Laser ultrasonic diagnostics of residual stress. Ultrasonics 2008; 48:631–5.
[32] Kinoshita M, et al. Weld piece visualization by laser-ultrasonic technique. Trans. Japan Soc. Mech. Eng. C. 2012;78:2824–36.
[33] Nomura K, Deno S, Matsuida T, Otaki S, Asai S. In situ measurement of ultrasonic behavior during lap spot welding with laser ultrasonic method. NDT E Int 2022; 130:102662.
[34] Scruby CB, Moss BC. Non-contact ultrasonic measurements on steel at elevated temperatures. NDT E Int 1993;26:177–88.
[35] Yu F, Saito O, Okabe Y. An ultrasonic visualization system using a fiber-optic Bragg grating sensor and its application to damage detection at a temperature of 1000 °C. Mech Syst Signal Process 2021;147:107140.
[36] Viktorov IA. Rayleigh and Lamb waves. Springer; 2013.
[37] Hayashi T. Plate dispersion pipe dispersion (Online) Available: http://www.nde.mech.eng.osaka-u.ac.jp/PlatePipeDispersion.htm. [Accessed 12 February 2023].